ASSESSING THE ACCURACY OF ROBOTIC JOINT REPLACEMENT USING VOLUME-BASED REGISTRATIONS

By

BRIAN PARK

A THESIS PRESENTED TO THE GRADUATE SCHOOL
OF THE UNIVERSITY OF FLORIDA IN PARTIAL FULFILLMENT
OF THE REQUIREMENTS FOR THE DEGREE OF
MASTER OF SCIENCE

UNIVERSITY OF FLORIDA

2011

To my wife and family

ACKNOWLEDGMENTS

I wish to express sincere appreciation and gratitude to Dr. Scott Banks, my advisor, whom gave me the opportunity to work with all the exceptional students and members from MAKO Surgical through this project. He gave me all the guidance and support needed to finish my thesis. I would like to thank Nick Dunbar, who has done work with MAKO Surgical, for all the training and support with previous projects; all of the skills, knowledge, and material used for those projects were essential to my master's thesis. I would like to thank Dr. Malisa Sarntinoranont for serving as a member of my committee.

Special thanks go to my wife and my family for all the physical, emotional, and spiritual support.

TABLE OF CONTENTS

page

LIST OF TABLES

LIST OF FIGURES

LIST OF ABBREVIATIONS

2D	Two-dimensional
3D	Three-dimensional
A/P	Anterior/Posterior (translation)
CT	Computed tomography
DOF	Degree of freedom
FLEX/EXT	Flexion/Extension (rotation)
INT/EXT	Interior/Exterior (rotation)
ITK	Insight toolkit
MI	Mutual information
M/L	Medial/Lateral (translation)
MR	Magnetic resonance (imaging)
PDF	Probability density function
post-op	Post operative
pre-op	Pre operative
RMS	Root mean square
S/I	Superior/Inferior (translation)
STD	Standard deviation
UKA	Unicompartmental knee arthroplasty
VAR/VAL	Varus/Valgus (rotation)
VTK	Visualization toolkit

Abstract of Thesis Presented to the Graduate School
of the University of Florida in Partial Fulfillment of the
Requirements for the Degree of Master of Science

ASSESSING THE ACCURACY OF ROBOTIC JOINT REPLACEMENT USING VOLUME-BASED REGISTRATIONS

By

Brian Park

August 2011

Chair: Scott A. Banks
Major: Mechanical Engineering

A volume-based 3D registration method was developed to assess the accuracy of robot-assisted knee implant placement in 20 patients who underwent robotic assisted unicompartmental knee arthroplasty. The volume-based registration uses pre- and post-operative CT scans registered with a mutual information cost-function. Voxelized pre-op model and post-op CT scans were registered to compare and measure the differences between the position and orientation of pre-op planned implants and the position and orientation of actual post-op femoral and tibial implants. RMS errors were used to measure the average alignment accuracy and dispersion. Results were compared with those obtained using global model-based 3D registration in a previous study. The volume-based registration produced similar results in less time. The RMS errors for femoral components were less than 1.5 mm and 3 degrees in all directions and less than 1.5 mm and 2.6 degrees for tibial components. A Bland-Altman assessment for agreement was done to compare results from the two registration methods. The two methods agree within 95% confidence limits. The volume-based registration method reduces registration time by almost 4 hours per bilateral knee study.

CHAPTER 1
BACKGROUND INFORMATION

Introduction

In medicine, it is not uncommon for a doctor to take images of a patient's treatment area more than one time using the same or different imaging modalities such as ultrasound, X-ray fluoroscopy, CT, or MR. High resolution, 3D, medical images like CT and MR images are widely used because they are capable of clearly showing many anatomical structures. Ultrasound or X-ray fluoroscopy is commonly used for guiding interventions and is "real-time", but only in 2D. They lack the spatial information and visibility to capture many important anatomical features contained or those that can be seen in CT and MR images. Since information gained from two images are usually of a complementary nature, proper integration is often needed to obtain useful data from the separate images. A first step in this integration process is referred to as registration. Registration of these medical images from different imaging devices has proven to be an important tool for extracting additional information for diagnosis, therapy, treatment planning, and surgery (Brown and Boult 1996, Maes et al. 1997, Lemiux et al. 1994, Pluim et al.2003, Roche et al. 2009).

Image registration is a fundamental step in all image analysis tasks in which information is gained from combining two or more images taken at different times (multi-temporal analysis) from different viewpoints (multi-view analysis), or from different sensors (multi-modal analysis) (Brown 1992, Zitova and Fluser 2003). It quantitatively relates the information in one image to information in another by aligning geometrically and transforming the data into one coordinate system. Registration is necessary in order to compare or integrate data obtained by different measurements. It is mostly

used in cartography, in remote sensing, in computer vision, and in medicine. In the last two decades, there have been a few comprehensive surveys of image registration methods that cover the relevant approaches and developments of registration techniques (Brown 1992, Maintz and Viergever 1998, Pluim et al. 2000 and 2003, Zitova and Fluser 2003). Over the years, a broad range of techniques have been developed for various types of data and problems, which are still used today.

Image Registration Method

According to previous research, image registration methods can be divided into four different subsections called preprocessing, measure, transformation, and implementation (Maintz and Viergever 1998, Pluim et al. 2003, Shams et al. 2010). During preprocessing, images are prepared or improved for registration. Typically, image processing is done to extract a region of interest or to remove noise using filters. The measure will be based on different types of metrics such as mean squares, normalized correlation, mutual information (MI), etc. The transformation can be classified as rigid (rotations and translations only), affine (rigid plus scaling and shearing), perspective (affine without preservation of parallelism of lines). Implementation includes interpolation, optimization and acceleration and other calculations that influence the results of the registration.

Preprocessing

In medical image registration the preprocessing can be divided into two categories: feature-based and intensity-based (Penney et al. 1998). Feature-based methods use salient features that have been segmented from each image for registration (Hill et al. 2000, Maurer Jr et al. 1996). They use a reduced amount of data but the segmentation stage is very hard to achieve automatically. Furthermore, manual

segmentation can be time consuming and errors in segmentation can lead to inaccuracies in the final registration. Intensity-based methods require little or no segmentation. They can directly compare voxels and pixels using measures based on image statistics, but typically are more computer-time consuming (Haber and Modersitzki 2006, Klein et al. 2010, Studholme et al. 1996).

Measure

There exist many types of metrics that can be used for image registration. Different registration metrics are more appropriate to use depending on the type and size of images that are to be registered. Out of all of the different types of metrics, MI has been shown to be most the popular registration measure because of its accuracy and robustness (Cizek et al. 2004, Kern and Pattichis 2007, Mattes et al. 2003, Pluim et al. 2000). Within MI, there are a few varieties of methods and types that have been implemented. For example, different definitions of entropy can be chosen when defining MI based on entropy, and different methods like Viola and Wells III, 1995 and Mattes et al., 2003 exist.

Transformation

For image registration, the applied transformation can be categorized according to the degrees of freedom (DOF) and further divided into rigid and non-rigid transformations. A transformation is defined to be rigid when it includes only translations and rotations. It is often used when registering images of rigid objects like bones. There have been many studies on rigid registration of images based on MI (Cizek et al. 2004, Maes et al., 2003, Thirion 1999).

Affine, perspective and curved transformations are non-rigid transformations. A transformation is called affine when an otherwise rigid transformation is allowed to

include shearing or scaling, which increases the DOF from six to twelve. Affine transformation preserves the parallelism of lines, but does not define angles, lengths or perspective. The curved transformations are like affine transformations but do not preserve the parallelism of lines. Non-rigid registrations are capable of dealing with more localized spatial changes and are the focus of current research and development (Andronache et al., 2008, Betke et al. 2001, Butz and Thiran, 2001, Klein et al. 2010). Non-rigid registrations are used when registering non-rigid objects such as human organs.

Implementation

Implementation involves interpolation, probability distribution estimation, and optimization. Interpolation usually is required for estimating the intensity value of a point when transforming points from one image to another. There are many ways to estimate using different interpolation methods like linear, partial intensity and cubic spline. Most commonly used methods to estimate probability distribution are by computing a joint histogram of intensities or using Parzen Windowing methods (Ibanez et al. 2005). An optimization is a numerical minimization routine used to find the lowest cost-function value, corresponding to the correct image registration.

Entropy

In information theory, entropy can be interpreted as a measure of uncertainty, variability, or complexity. In 1948, Shannon introduced a measure that uses the probability density function (PDF) as an information weight for every outcome. This was done assuming that all outcomes are not equally likely to occur. Shannon's entropy is defined as,

$$H = \sum_i p_i \log \frac{1}{p_i} = -\sum_i p_i \log p_i . \quad (1\text{-}1)$$

where H is the entropy of a random variable, *i*, and p_i is the PDF. To compute a PDF, Mattes et al. uses Parzen Windows method, also know as kernel density estimator with B-spline functions instead of Gaussian function used by Viola and Wells (Ibanez et al., 2005, Mattes et al. 2003).

Mutual Information

Definition

MI measures how much information one random variable indicates/represents about another random variable. When used to compare medical images, the random variables are the intensity values of the images. The spatial transformation that maximizes the MI over the transformations parameter T is,

$$\hat{T} = \arg\max_T I(u(x), v(T(x))), \quad (1\text{-}2)$$

where I is the MI and u(x) is the reference (first) image with random variable x and v(T(x)) is the floating (second) image with random variable x after it is spatially transformed by an operator T (Viola and Wells III, 1995 and1997, Pluim et al. 2003).

MI is defined in terms of entropy and shown in the equation below.

$$I(u(x), v(T(x))) = H(u(x)) + H(v(T(x))) - H(u(x), v(T(x))) \quad (1\text{-}3)$$

Where H(u(x)) and H(v(T(x)) are the entropy and H(u(x),v(T(x))) is the joint entropy of u(x) and v(T(x)).

Mattes et al. Implementation

For Mattes et al. implementation, I in (Eq.1-2) is minimized and only one set of intensity sample is drawn from the image and it is used to evaluate the marginal and

joint PDF (Eq. 1-4). The PDF is evaluated at uniformly spread bins along the respective dimensions of the joint histogram of the fixed and moving images. Entropy values are computed by summing over all the bins. To smooth the marginal histogram for the fixed image, a zero order (boxcar) B-Spline kernel, $\beta^{(0)}$, is used for computing the PDF (Eq. 1-5) and a third order B-spline kernel, $\beta^{(3)}$, is used to compute the PDF of the moving image (Eq. 1-6) (Mattes et al. 2003).

$$p_{k,i} = \alpha \sum \beta^{(0)}(k - \frac{u(x) - u^0(x)}{\Delta b_u}) * \beta^{(3)}(i - \frac{v(T(x)) - v^0(x)}{\Delta b_v}) \tag{1-4}$$

$$p_v(k) = \sum \beta^{(0)}(k - \frac{u(x) - u^0(x)}{\Delta b_u}) \tag{1-5}$$

$$p_v = \sum p_{k,i} \tag{1-6}$$

where, k is the integer value indexed from zero to the specified number of bins for the fixed image and i from zero to the number of bins for the moving image. The normalization factor is α and each contributing image value is normalized by the minimum intensity value, $u^0(x)$ or $v^0(x)$, and by the intensity range of each bin, Δb_u or Δb_v. This is done to fit the contributing image value into the specific number of bins for the fixed and moving images intensity distribution (Mattes at al. 2003).

The negative of mutual information is used and it is represented as show below.

$$I = -\sum_i \sum_k p_{k,i} \log \frac{p_{k,i}}{p_u p_v} \tag{1-7}$$

A B-spline kernel is used instead of Gaussian kernel because it has a finite support region where each intensity sample only affects a small number of bins and, thus, is less computationally intensive (Ibanez et al, 2005).

Optimization

The Amoeba optimization routine was chosen for this work [ref]. Amoeba is also known as the Nelder-Meade downhill simplex method, or the flexible polyhedron method. It starts by forming an initial simplex from N+1 test points. A simplex is a polytope of N+1 vertices in N-dimensions, a tetrahedron for a 3D space (Nelder and Mead, 1965). At every iteration, new points are computed along with their function value at the test points. It replaces the worst of the test points with a point determined by reflecting the worst point through the centroid of the remaining N points. The algorithm tries to expand exponentially along this line if the new point is better than the current best point, and form a new simplex. However, if the current point is still the best point, then it shrinks the simplex towards the best point and, finally, the minimum (Patil and Ravi, 2005).

Reflection, contraction, or expansion processes are used at each iteration. After an initial simplex is created, a reflection process is used for calculation of the next point, P_n, using the following equation:

$$P_n = (1+\alpha)\overline{P} - \alpha P_{high} \tag{1-8}$$

where α is a positive constant reflection coefficient and P_n is on the line that joins P_{high} and $\overline{P}$. P_{high} is the highest value from the initial simplex points and $\overline{P}$ is the centroid. If, P_n lies between P_{low} and P_{high} then P_n replaces P_{high} and the process is repeated with new simplex. If P_n is higher than P_{high}, then the new next point, P_{n+1}, is found using the expansion process with a positive constant expansion coefficient, γ, as shown in Eq. 1-9. However, if after the reflection process, P_n is lower than P_{low}, the new next point is

found using a contraction process with contraction coefficient, β (Eq. 1-10). This is repeated until the convergence criteria are met.

$$P_{n+1} = \gamma P_n + (1-\gamma)\overline{P} \tag{1-9}$$

$$P_{n+1} = \beta P_h + (1-\beta)\overline{P} \tag{1-10}$$

Mattes MI was used for the intensity-based image registration process in this study. An Euler's 3D transformation was used because it is a rigid transformation and uses Euler's angles, a more user-friendly routine than direct use of 4x4 homogeneous transformation matrices. For implementation, the linear interpolator and Amoeba optimizer were used.

CHAPTER 2
VOLUME-BASED 3D REGISTRATION

Introduction

Image registration is a fundamental step in all image analysis tasks in which information is gained from combining two or more images taken at different times, views, or from different sensors. This is an essential process for extracting additional information for diagnosis, therapy, treatment planning, and surgery in the medical field. Robot-assisted unicompartmental knee arthroplasty is one of many surgeries that use image registration (Roche et al., 2009, Fueziec et al., 1998) for treatment planning and surgery. Image registrations are also used when analyzing the images taken before and after the surgery for post-op, assessment.

The data used for this study was previously analyzed for accuracy of robot-assisted UKA. One surgeon performed dynamic tactile-guided unilateral medial UKA with robotic-assisted bone preparation on 20 patients (TGS^{TM}; MAKO Surgical Corp. Fort Lauderdale, FL). A global model-based 3D registration, a feature-based method, was used for assessment. The position and orientation of the surgically placed implants were calculated relative to the planned implant positions and orientations set during the pre-op planning process. This process was validated, and the measurements were within 1 mm and 2 degrees in all directions for the femoral and tibial components. However, since it was a feature-based method, a segmentation process was needed in order to do the registrations, and this process took about 5 hours per bilateral pair of knees. During this study, an intensity-based method was used which eliminated the segmentation process and dramatically reduced the overall analysis time.

Materials And Methods

For this study, 20 knees (19 patients, 1 bilateral) were used for analysis. Of these patients, 9 were male and 10 were female with ages ranging from 49 to 92 years, height ranging from 155 to 185 cm, weight ranging from 44 to 111 kg, and body mass index ranging from 23 to 33. Pre-operative and post-operative CT-scans had approximately 200 slices taken through the knee with a slice thickness of 1 mm. The pre-op model and post-op CT scans were compared to quantify the differences between the pre-op planned implant positions and the actual post-op femoral and tibial implant positions.

An intensity-based method is used for 3D image registration in this study. This requires the reference data set (the pre-operative plan) and the outcome data set (the post-operative CT scan) to be represented as 3D volume images. The pre-operative plan utilized a 3D polygonal-surface model which was voxelized in order to permit direct 3D registration with the post-operative CT data set.

Voxelization

Voxelization is the process of representing continuous geometric objects as a set of voxels that best approximate the continuous object (Petil, 2005). One method for voxelization is ray-tracing, where the overall 3D image result is the combination of orthographic projections from each x, y, and z direction. After a regular grid of N x N x N voxels is placed over the object domain, a series of rays are projected to intersect the object. A binary decision is made as to whether each voxel is on, inside, or outside of the object (Petil, 2005), with corresponding intensity values assigned. The voxel intensity is set to be 1 when it is on and inside the object, and zero when it is outside the object. The voxel depth is set to be the same as the CT slice thickness, 1 mm, and the voxel sizes are set to be the same as the CT in the x and y directions, 0.488281 mm.

Volxelization was performed using a Matlab program developed by Aitkenhead in 2010 (www.mathworks.com/matlabcentral). After voxelization, the stacks of voxel layers are represented in binary and stored as 16-bit raw data using an image program called ImageJ (http://rsb.info.nih.gov/ij/).

Registration

The image registration was performed using medical image processing and visualization software called MeVisLab (developed by Fraunhorer MEVIS, and Mevis medical solutions, www.mevislab.de) (Figure 2-1-A). MeVisLab has a modular framework that is user friendly and has built-in ITK and VTK modules (Figure 2-1-B). Registration was performed using the ITK Mattes MI metric, ITK Euler's 3D transformation, ITK linear interpolate image, and ITK Amoeba optimizer modules in MeVisLab. The parameters used in Mattes MI metric are shown in Table A-1.

Within ITK Mattes MI metric module, a clamp out tool can be used to extract specific ranges of intensity values, so that only values from the desired range are used for analysis. This tool is particularly helpful in reducing disturbances caused by near surroundings during registration, since the intensity values of the bones and the implants are very different, but are located next to each other and surrounded by tissues. The intensity values of bones range from 1000 – 2600, tissue from 950 – 1100, femoral component from 3900 – 4000, and polymeric tibial component from 850-950. The intensity values of bones and tissue overlap but the outer surface of the bones has a minimum intensity value of 1400. Therefore, if the initial guess of the moving image is close enough to the fixed images, the intensity values of the tissues have minimal effect on the registration.

Manual registration is done first to reduce the computational time and to increase the success rate of the optimizer converging to the optimal result. This process is done using the ITK Euler's 3D transformation module. It allows the user to input initial location in mm and rotations in radians, and converts the measurements to 4x4 homogeneous transformation matrices. After changing x, y, z translations and rotations, and placing the moving and fixed images as close as possible, the optimizer is used to find the optimal solution.

The ITK Amoeba optimizer model has eight parameters that the user can change to customize the optimizer for any use. Only a few parameters were changed for registering different components. For registering the femoral and tibal components, the maximum number of iterations was set to 2000, the parameter convergence tolerance was set to 0.25 voxel, and the cost function convergence was set to 0.005% (Table A-2). For registering bones the same parameters were used except the maximum number of iterations were set as 500.

Calculations

When opening the images in MeVisLab, as default, the origin of the entire reference frame is moved to a top, left corner of the bottom image, not to the image center as one might expect. Also, during the voxelization process, the origin is moved when a grid is placed over the polygonal model (Fig. 2-2). This translation of the origin is accounted for in the final calculation and all displacements are quantified using 4x4 homogeneous transformation matrices. The actual implant placements are calculated by taking the measured surgically placed implant position with respect to the plan placement (Eq. 2-1). The measured implant position is the position of the implant relative to the position of the bone (Eq. 2-2) and it is found using the relative position of

the implant and the bone (Eq. 2-3, Eq. 2-4). Proper transformation matrix calculations are graphically shown in the Figure 2-3.

$$T_{Actual} = {}^{\text{Pre-opBone}}_{\text{Pre-opImplant}}T_{Measured} * inv(T_{Planned}) \quad (2\text{-}1)$$

$${}^{\text{Pre-opBone}}_{\text{Pre-opImplant}}T_{Measured} = {}^{\text{Pre-opBone}}_{\text{Post-opCT}}T * inv({}^{\text{Pre-opImplant}}_{\text{Post-opCT}}T) \quad (2\text{-}2)$$

$${}^{\text{Pre-opImplant}}_{\text{Post-opCT}}T = {}^{\text{Pre-opImplant}}_{\text{VoxelImplant}}T * {}^{\text{VoxelImplant}}_{\text{Post-opCTImplant}}T * inv({}^{\text{Post-opCT}}_{\text{Post-opCTImplant}}T) \quad (2\text{-}3)$$

$${}^{\text{Pre-opBone}}_{\text{Post-opCT}}T = {}^{\text{Pre-opBone}}_{\text{VoxelBone}}T * {}^{\text{VoxelBone}}_{\text{Post-opCTBone}}T * inv({}^{\text{Post-opCT}}_{\text{Post-opCTBone}}T) \quad (2\text{-}4)$$

RMS errors were used to quantify the average alignment accuracy and dispersion. Bland-Altman plots were used to compare the 3D registration results with those achieved from surface registration in the previous study.

Results and Discussion

The absolute values of implant error for the femur and tibia implants are shown in Figure 2-4 and Figure 2-5. For tibia implant placement, there is an outlier and it is unused for analysis, as it was neglected in the previous study (this outlier resulted from the surgeon using the robot system for demonstrations AFTER the surgery was completed). The calculated RMS errors for femoral component placement were under 1.5 mm and 3° in all directions of the planned implant position (Table 2-1). RMS errors for tibial component placement were also under 1.9 mm and 2.6° in all directions (Table 2-2). Since a validation study was not done for this method, the data collected were compared to the results from the previous study. RMS errors resulting from 3D image registration are less in A/P translation and all the rotations for femur implants, and in A/P translation and VAR/VAL and INT/EXT rotations for tibia implants (Table 2-3, Table 2-4). A Bland-Altman analysis was used to evaluate the level of agreement between the two registration methods (Bland and Altman, 1986). A range of agreement was defined

as mean bias ±2 Standard deviation (STD) for every translation and rotation for both femoral and tibial components. The mean and STD of the result differences (Table 2-5, Table 2-6) were used for the Bland-Altman plots. Mean, ±2 STD and trend lines are also shown (Figure 2-6 – 2-17). All the plots indicate that the there is 95% limits of agreement except for M/L and S/I translation in femur implant and INT/EXT rotation for tibia implant.

Implant placement errors represent the total error resulting from surgery and measurement, and there likely are contributions from voxelization, registration, and mathematical imprecision. To reduce rounding error in all the measurements, six decimal places were carried out through all the calculations. As discussed by Patel and Ravi, 2005, errors during voxelization are smaller with higher spatial resolution and voxel numbers, but because voxel size and depth were set to be the same as post-op CT scans, the resolution could not be changed. Some voxelization error could be eliminated if the pre-op CT scans could be used, but that would require the additional step of aligning coordinate systems between the CT data set and the pre-operative plan. This will also reduce final computational time and possibly be more accurate since the volume-based registration is needed only for the femur and tibia implants.

Errors during registration can be caused by numerous things, such as the parameter choices in the MI metric and the optimizer. Parameter values in the Amoeba optimizer may not be the optimal values, but this was not investigated. One problem faced during optimization was the optimizer not converging to a unique solution. This could be due to convergence problems of the Nelder-Mead algorithm (Lagarias et al. 1998, and Mckinnon, 1999). This could be due to not having the necessary parameter

values, because researcher like Cizek et al., 2004 found Nelder-Mead algorithm to be fast and robust.

Even with these uncertainties, the quantified volume-based registration RMS errors for the femoral and tibial component placement were less than the global model-base registration RMS errors. However, a validation study was not done with this method, so it cannot be stated that one is more accurate than the other. Errors from the volume-based method are similar to those from the model-based method, but with much shorter computational and user time since the segmentation process was eliminated. The registration times are about the same, even with the additional time spent during the voxelization process. Overall, almost 4 hours were saved per bilateral pair of knees using a computer with 2.4 GHz processor (Table 2-7).

MeVisLab software was chosen out of many existing medical imaging and visualization programs because it has ITK and VTK built in, and a modular framework that is user friendly. Although it is very compatible with Python and Java, the software does not require scripting or programming skills. Another reason for using this program was it is free. However, a drawback in using this program is that not all the registration metrics, transformations, and optimizers work properly. The developers are still in the process of improving and correcting exiting bugs in the software. The program also uses modules that are easy to work with even though users are not able to control all the calculations and activities. Additional Python or Java programming skills can allow further control for users.

A validation study will be very helpful in determining whether the volume-base registration is more accurate than global model-based registration. Also, by obtaining

the information on the reference frame used in pre-op planning, will eliminate another process from volume-based registration and reduce errors in the final registration. Hypothetically, the volume-based registration should be the more accurate than global-based registration because it reduces a source of uncertainties and errors. Also, finding the optimal parameter values for the optimizer will reduce errors and uncertainties as well as improve the convergence rate. These improvements will not only reduce error and computational time but also increase the confidence in the results.

Conclusion

This paper has compared the accuracy of the knee implant placements using data from a 20 patient cohort who had robotic-assisted UKA. The accuracy assessment was performed using a volume-based 3D registration with Mattes et al. MI, 3D Euler's transformation, linear interpolator, and an Amoeba Optimizer, registering 3D post-op CT scan and voxelized pre-operative model. The results were compared with results from global model-based 3D registrations done in the previous study.

RMS errors for the femoral and tibial component placement relative to the planned were less using the volume-based 3D registration process. Although this is the case, a validation study was not done with this method so it cannot be concluded that one is more accurate than the other. However, the volume-based registration can produce similar results as global model-based registration with 95% limits of agreement in dramatically less time.

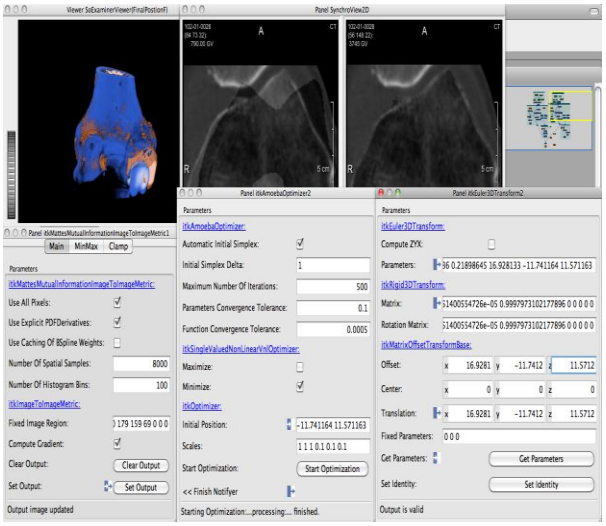

A

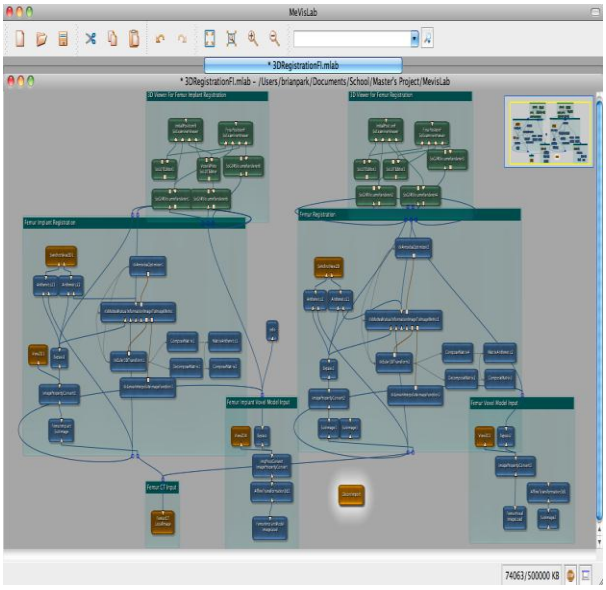

B

Figure 2-1. A) A snapshot of a running registration. B) A snapshot of module framework of MeVisLab software.

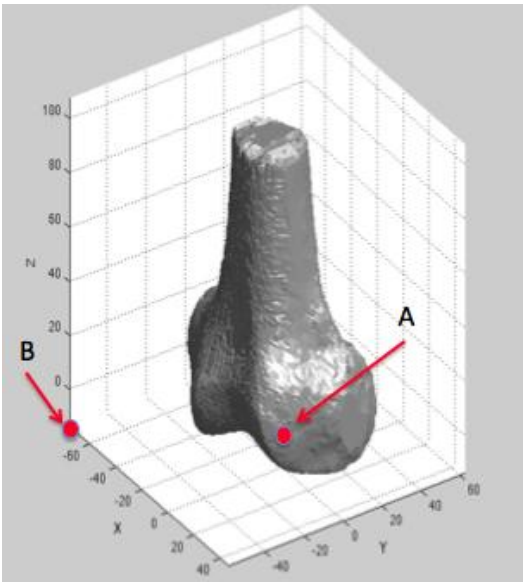

Figure 2-2. Coordinate system definition for one of the femur with origin at point A. After the voxelization the origin will move to point B.

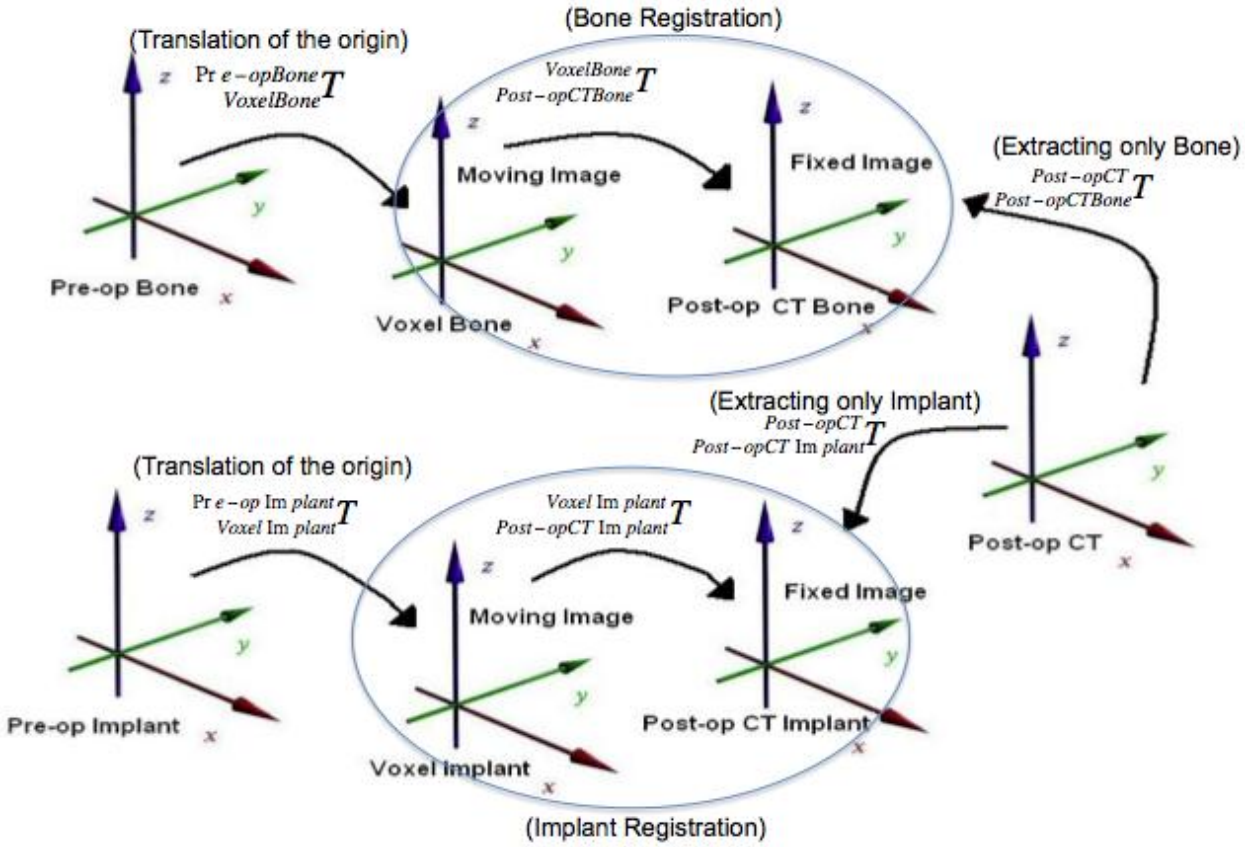

Figure 2-3. Graphical representation of the implant position calculation.

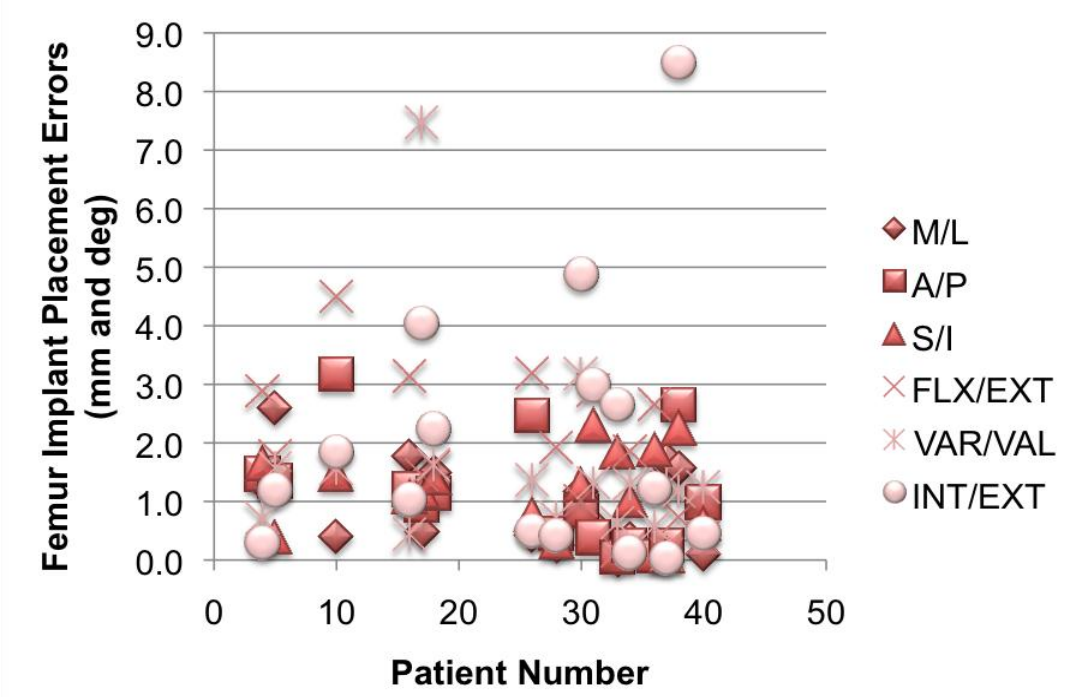

Figure 2-4. Absolute values of implant placement errors for the femoral component

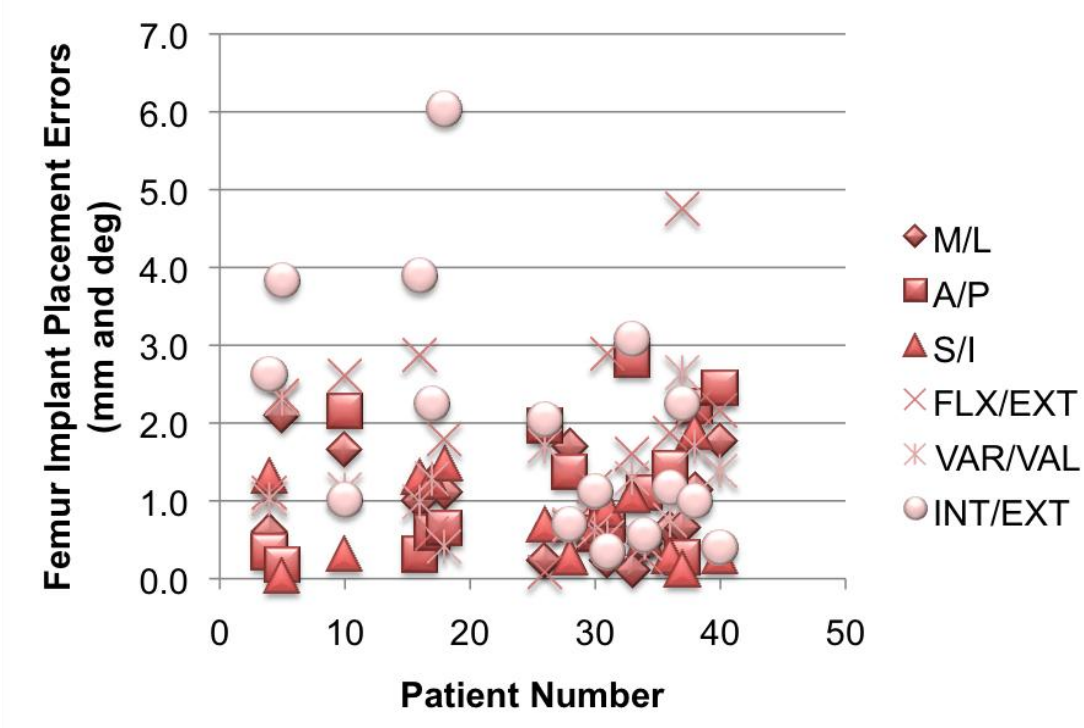

Figure 2-5. Absolute values of implant placement errors for the tibial component

Table 2-1. Femur implant placement errors using volume-base registration (mm and deg)

Patient	M/L	A/P	S/I	FLX/EXT	VAR/VAL	INT/EXT
4	1.30	-1.46	-1.64	-2.88	0.70	0.29
5	2.59	1.34	0.38	1.77	-1.56	-1.18
10	-0.40	-3.16	-1.46	-4.50	1.54	-1.84
16	1.76	-1.20	-1.07	-3.13	-0.43	-1.02
17	-0.48	-0.93	-1.16	-1.45	7.46	-4.04
18	1.48	-1.13	-1.40	-1.59	1.62	-2.23
26	0.42	-2.46	-0.76	-3.18	1.36	-0.49
28	-0.24	-0.45	-0.30	-1.91	0.72	-0.41
30	1.16	-0.82	-1.28	-1.01	3.17	-4.87
31	0.60	0.38	-2.30	-2.89	-1.30	-2.97
32	0.21	1.20	0.76	2.77	2.82	-1.24
33	0.00	-0.04	-1.84	-0.13	0.62	-2.65
34	0.35	0.24	-1.00	-1.85	1.28	0.11
36	1.26	-0.07	-1.88	-2.65	0.56	-1.20
37	1.70	-0.25	0.07	0.09	-1.28	0.03
38	1.57	2.64	2.24	0.73	1.16	-8.49
40	-0.09	0.98	0.60	0.37	1.24	-0.45
Mean	0.77	-0.30	-0.71	-1.26	1.16	-1.92
STD	0.90	1.43	1.18	1.95	2.09	2.23
RMS	1.19	1.46	1.38	2.32	2.39	2.94

Table 2-2. Tibia implant placement errors using volume-base registration (mm and deg)

Patient	M/L	A/P	S/I	FLX/EXT	VAR/VAL	INT/EXT
4	0.60	0.34	1.32	-1.09	1.02	2.62
5	2.10	0.17	0.03	-2.34	2.30	3.83
10	-1.65	2.15	0.31	-2.59	1.14	-1.00
16	-1.00	-0.31	1.30	-2.86	-0.98	3.88
17	1.23	0.59	1.24	-0.57	-1.28	-2.24
18	1.10	0.65	1.47	1.79	0.41	-6.03
26	-0.23	1.97	0.69	-0.08	-1.70	2.04
28	-1.69	1.37	-0.27	-0.66	0.69	0.69
30	0.76	0.57	0.68	-1.17	0.61	-1.11
31	0.23	0.69	-0.88	-2.88	0.53	0.34
32	0.22	5.01	0.84	2.38	-4.30	-29.24
33	-0.11	2.81	1.07	1.59	1.28	3.08
34	0.44	1.10	-0.53	-0.27	-0.44	-0.54
36	-0.63	1.42	0.29	-1.86	0.74	-1.16
37	0.65	-0.27	0.12	-4.74	-2.64	-2.25
38	1.14	2.22	1.88	-2.20	-1.69	0.99
40	-1.76	2.44	0.29	2.15	-1.37	-0.39
Mean	0.08	1.35	0.58	-0.91	-0.33	-1.56
STD	1.12	1.33	0.75	2.01	1.67	7.56
RMS	1.12	1.89	0.95	2.20	1.71	7.72
Mean*	0.07	1.12	0.56	-1.11	-0.09	0.17
STD*	1.15	0.97	0.77	1.88	1.37	2.60
RMS*	1.16	1.48	0.95	2.19	1.37	2.61

* indicates the values calculated with measured data from patients 32 neglected.

Table 2-3. The RMS values for volume-base and global model-base registration for femur implants

RMS	M/L	A/P	S/I	FLX/EXT	VAR/VAL	INT/EXT
Volume-based	1.18	1.45	1.37	2.32	2.38	2.94
Global model-based	1.06	1.57	1.20	2.37	2.74	3.08

Table 2-4. The RMS values for volume-base and global model-base registration for tibia implants

RMS	M/L	A/P	S/I	FLX/EXT	VAR/VAL	INT/EXT
Volume-based	1.16	1.48	0.96	2.19	1.38	2.61
Global model-based	0.99	1.73	0.69	2.01	1.57	2.86

Table 2-5. Differences in error between the placement errors of femur implant found using volume-based registration and global model-based registration (mm and deg).

Patient	M/L	A/P	S/I	FLX/EXT	VAR/VAL	INT/EXT
0004	0.32	-0.40	-0.92	-0.75	-0.59	0.84
0005	0.08	1.10	0.14	1.25	-0.86	0.47
0010	0.06	0.31	-0.24	0.89	-1.07	-0.09
0016	0.59	0.94	0.41	1.65	0.03	0.92
0017	-0.10	-0.36	-0.38	0.69	-0.64	-0.79
0018	0.32	-0.38	-0.99	-0.93	-1.24	-0.25
0026	0.01	-0.36	-0.42	0.55	-0.11	0.87
0028	-0.16	-0.51	0.32	-0.75	-0.86	0.63
0030	0.17	-0.25	-0.39	-0.21	-0.60	-0.44
0031	0.15	0.42	-0.24	-0.86	-0.19	-0.78
0032	-0.21	-0.04	1.66	0.66	-0.13	-0.92
0033	0.21	-0.58	-1.09	0.05	-1.35	-0.19
0034	0.02	-1.21	-0.30	-1.34	-0.28	0.59
0036	0.22	0.05	-0.15	-0.87	-0.83	0.80
0037	-0.14	0.70	-0.14	1.28	-1.55	1.18
0038	0.25	-0.68	-0.56	0.44	-0.21	1.17
0040	0.63	0.53	1.13	-0.36	0.04	0.37
Mean	0.14	-0.04	-0.13	0.08	-0.61	0.26
STD	0.24	0.63	0.71	0.92	0.50	0.71
RMS	0.28	0.63	0.72	0.92	0.79	0.75

Table 2-6. Difference in error between the placement errors of tibia implant found using volume-based registration and global model-based registration (mm and deg).

Patient	M/L	A/P	S/I	FLX/EXT	VAR/VAL	INT/EXT
4	-0.61	0.20	1.25	-0.23	0.01	-0.82
5	0.89	-0.60	1.21	-0.90	-0.60	-0.29
10	-0.39	0.75	-0.08	-1.07	0.04	-0.70
16	-0.79	-0.30	1.20	-1.04	-0.30	-0.95
17	0.54	-0.49	0.58	-0.86	1.40	0.26
18	-0.26	-0.70	-0.05	1.30	0.65	-0.25
26	0.06	-0.26	-0.25	1.18	0.73	0.15
28	-1.08	-1.52	-0.05	1.68	-1.29	-0.93
30	0.96	-0.31	0.43	0.28	1.21	-0.90
31	0.31	0.71	-0.57	0.75	-0.45	0.01
32	0.44	-1.28	0.53	0.26	0.95	1.69
33	0.51	1.31	0.95	0.14	0.97	-1.37
34	0.32	-0.49	-0.83	0.03	-0.29	-0.36
36	-0.55	1.12	-0.11	-0.44	0.84	0.44
37	0.84	-0.84	-0.19	-1.62	-0.11	-0.71
38	-0.45	-1.35	0.65	0.62	-1.13	1.26
40	0.29	-0.60	0.30	-0.80	-0.43	-0.68
Mean	0.06	-0.27	0.29	-0.04	0.13	-0.24
STD	0.63	0.84	0.63	0.95	0.81	0.81
RMS	0.63	0.88	0.69	0.95	0.82	0.85

Table 2-7. Estimated time for global model-based and volume-based registration.

Process	Global Model-Based Registration (per bilateral knees)	Volume-Based Registration (per bilateral knees)
Segmentation	5hrs	0hrs
Preparation/voxelization	5 minutes	20 minutes
Registration	1hr	2 hrs
Data processing/recording	5 minutes	5 minutes
Total	6hrs and 10 minutes	2 hrs and 25 minutes

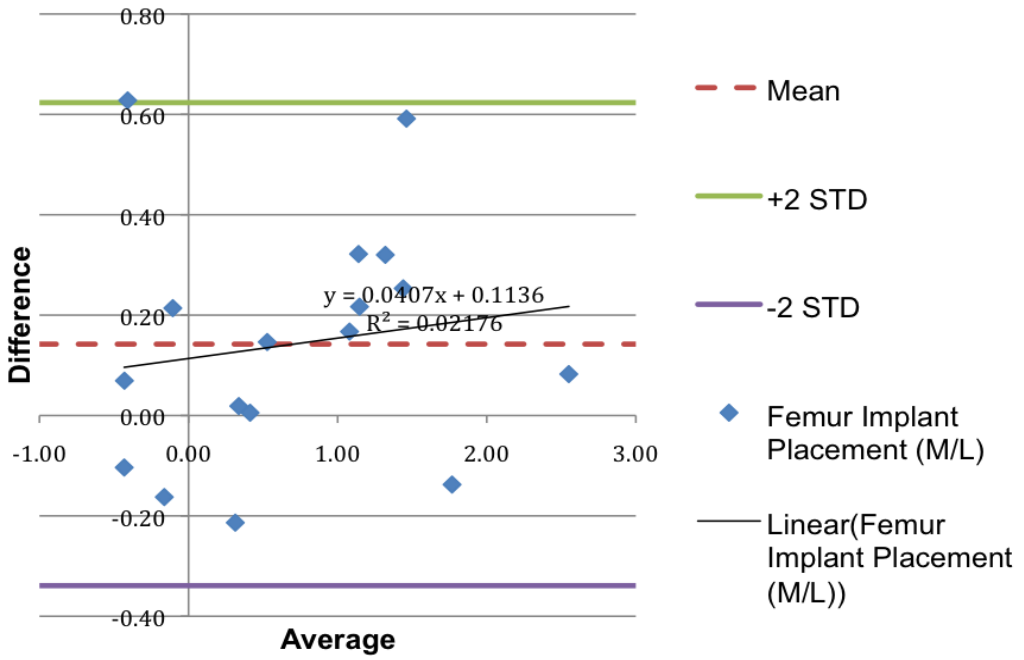

Figure 2-6. Bland Altman plot of femur implant placement in M/L translation.

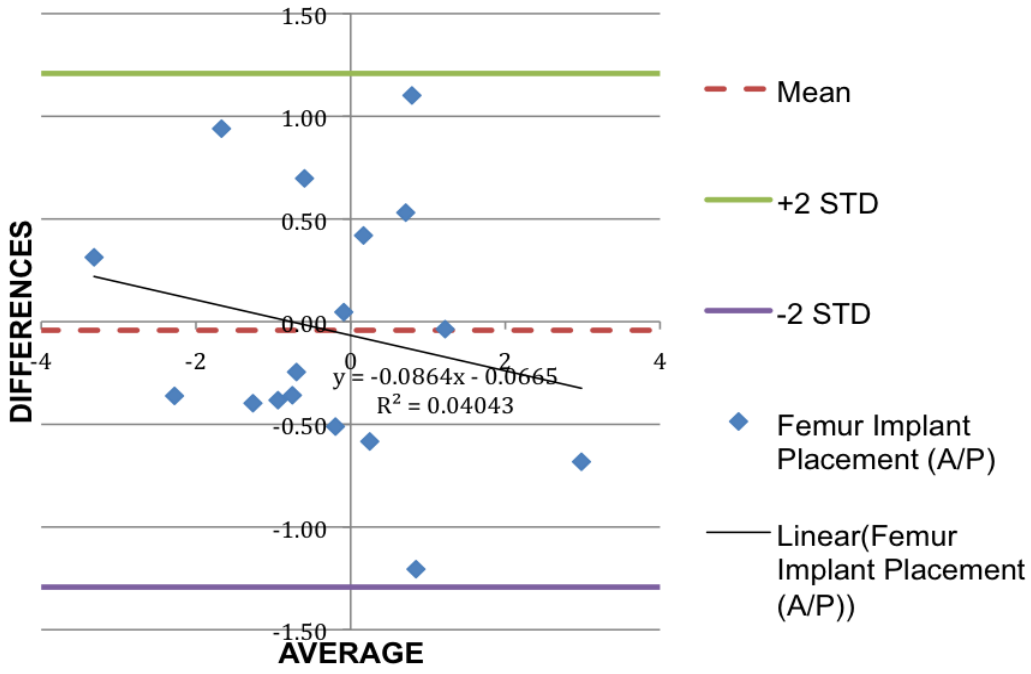

Figure 2-7. Bland Altman plot of femur implant placement in A/P translation.

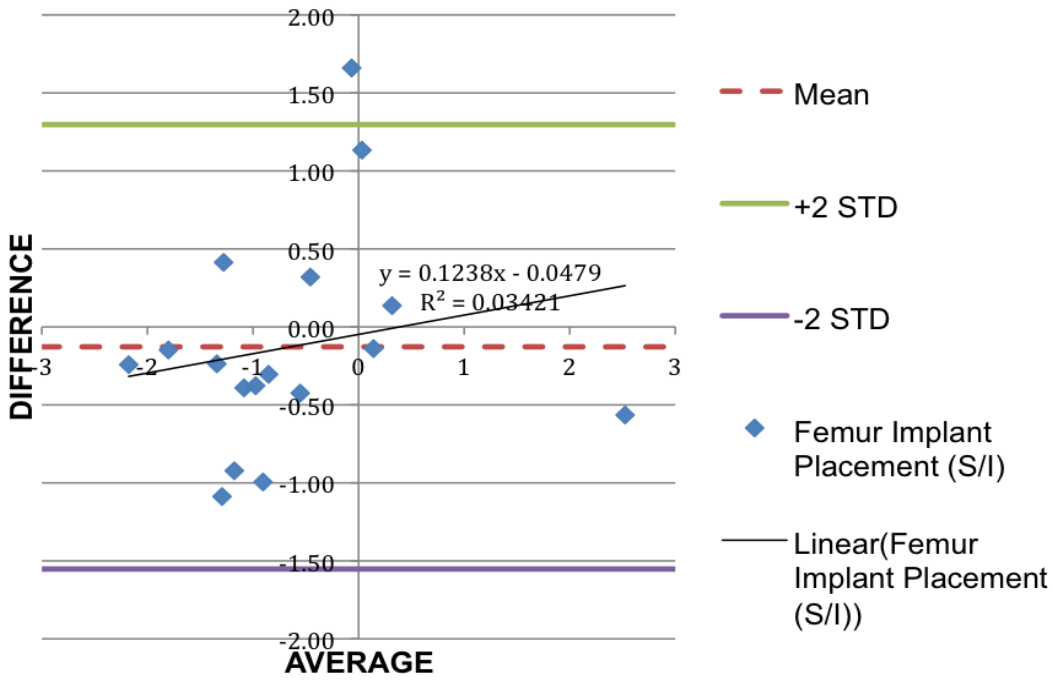

Figure 2-8. Bland Altman plot of femur implant placement in S/I translation

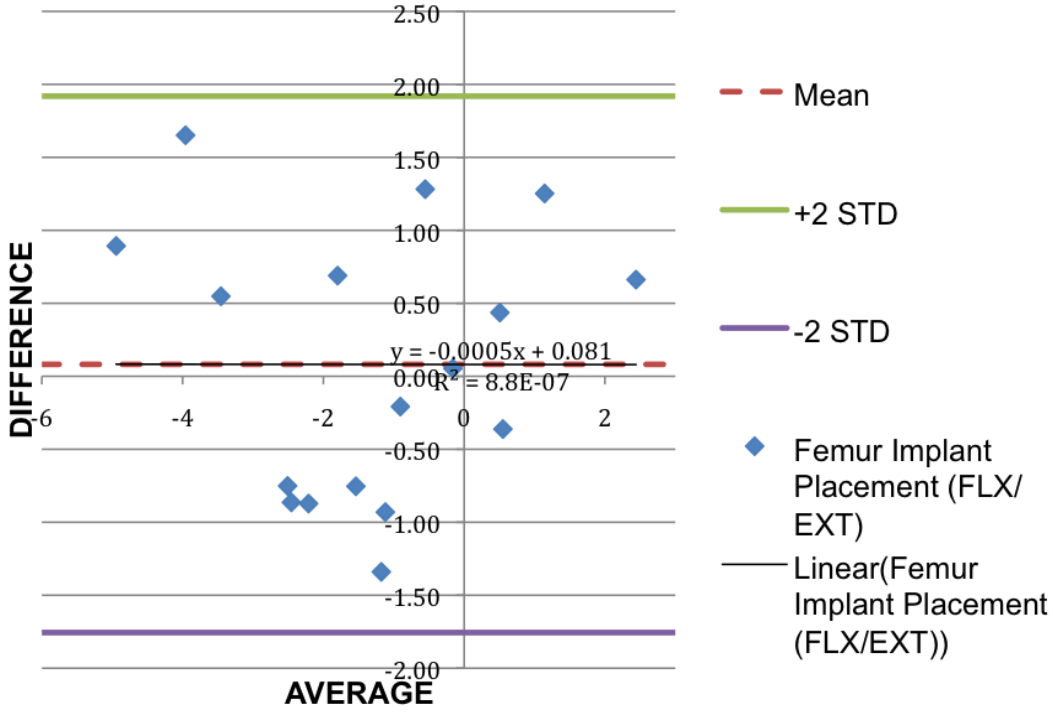

Figure 2-9. Bland Altman plot of femur implant placement in FLX/EXT rotation.

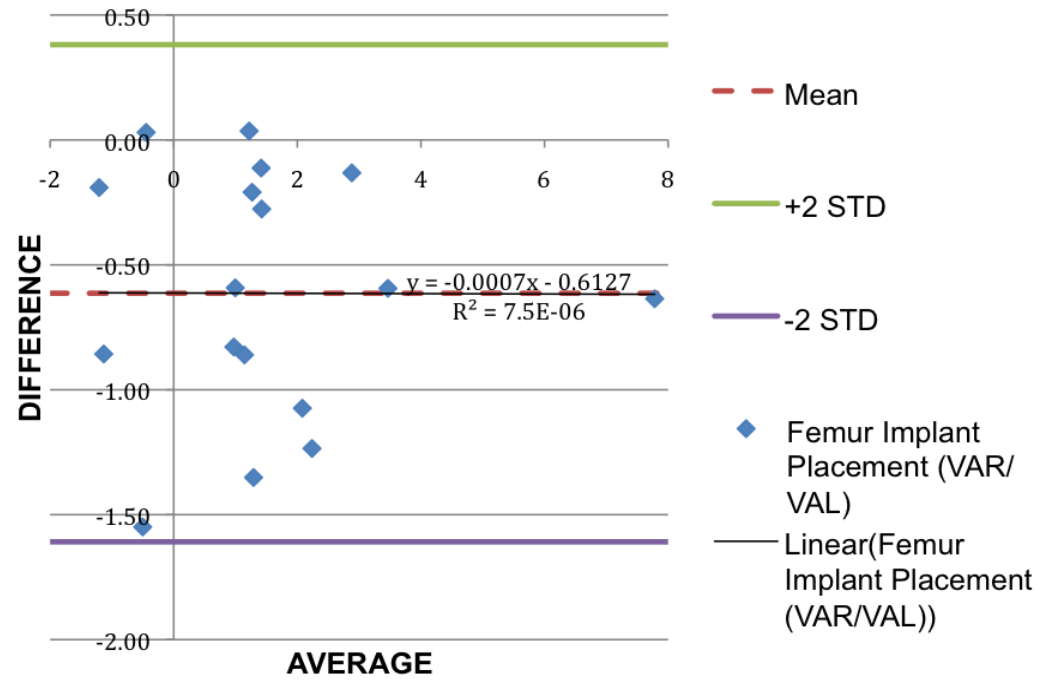

Figure 2-10. Bland Altman plot of femur implant placement in VAR/VAL rotation.

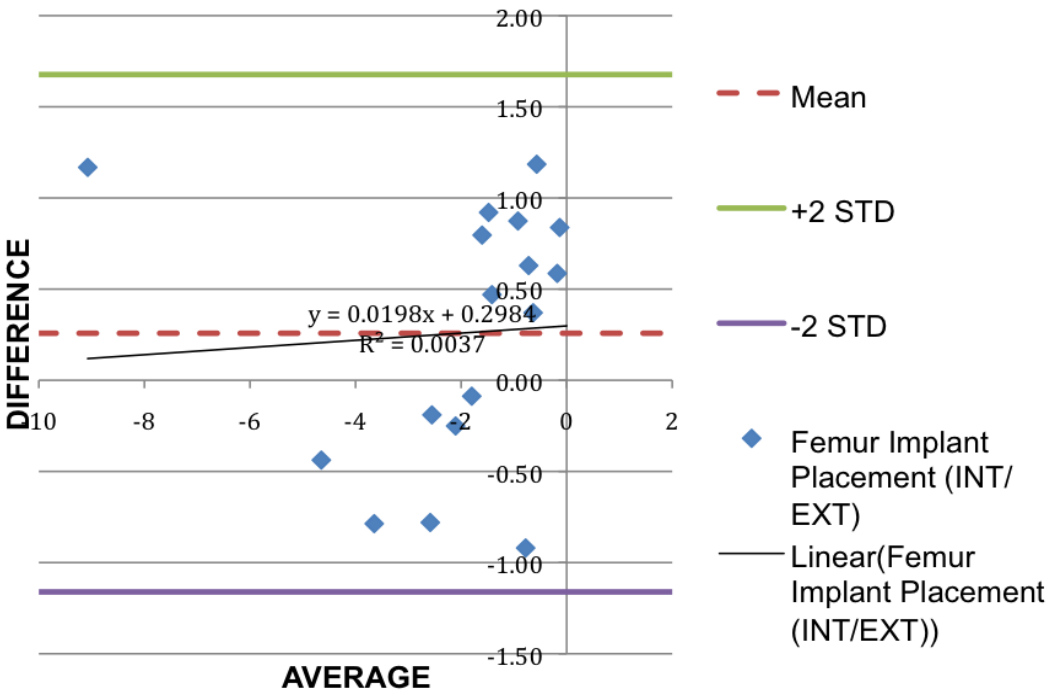

Figure 2-11. Bland Altman plot of femur implant placement in INT/EXT rotation.

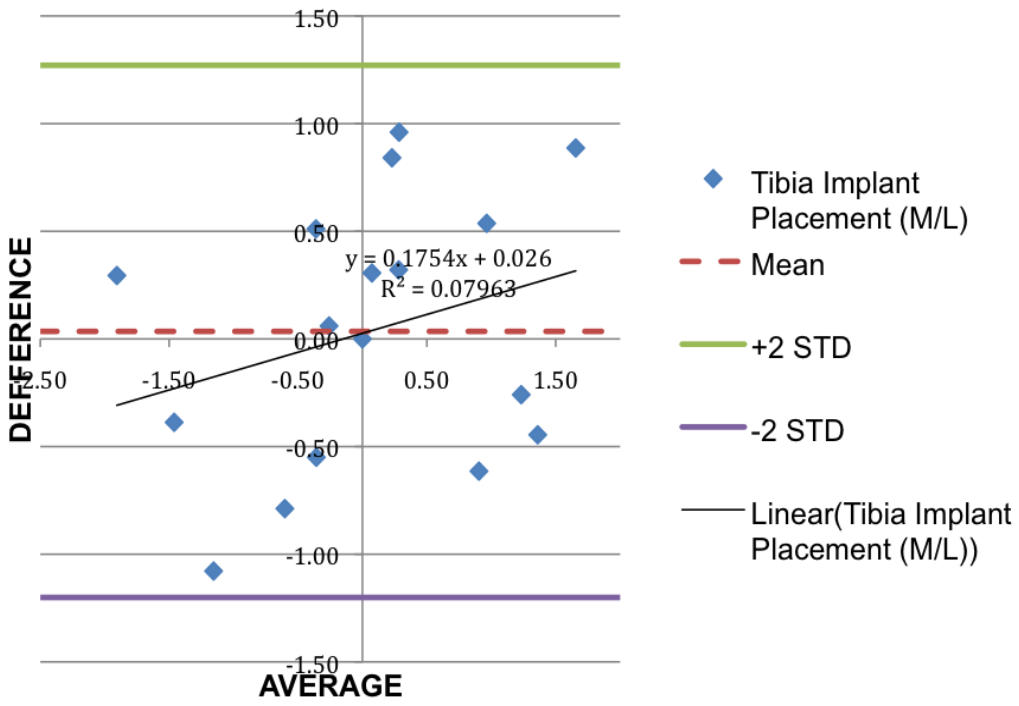

Figure 2-12. Bland Altman plot of tibia implant placement in M/L translation.

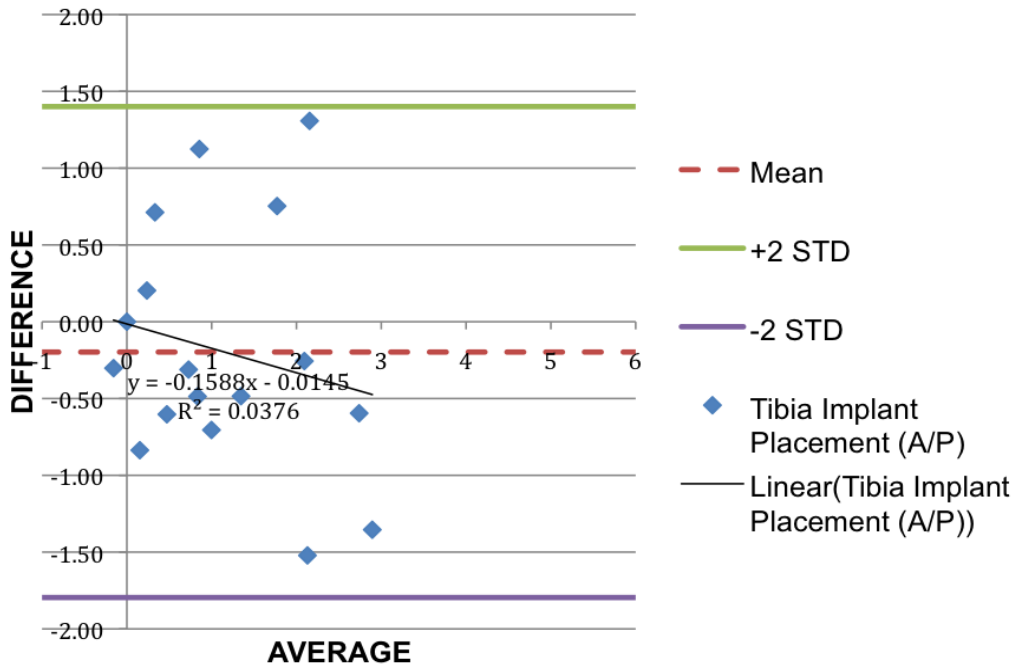

Figure 2-13. Bland Altman plot of tibia implant placement in A/P translation.

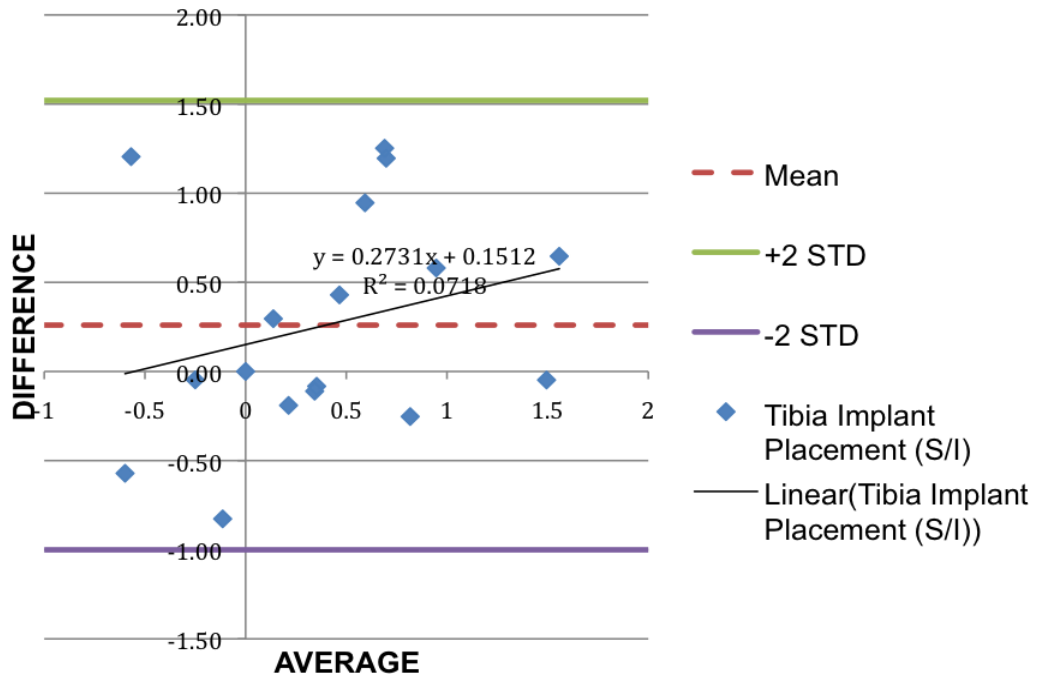

Figure 2-14. Bland Altman plot of tibia implant placement in S/I translation.

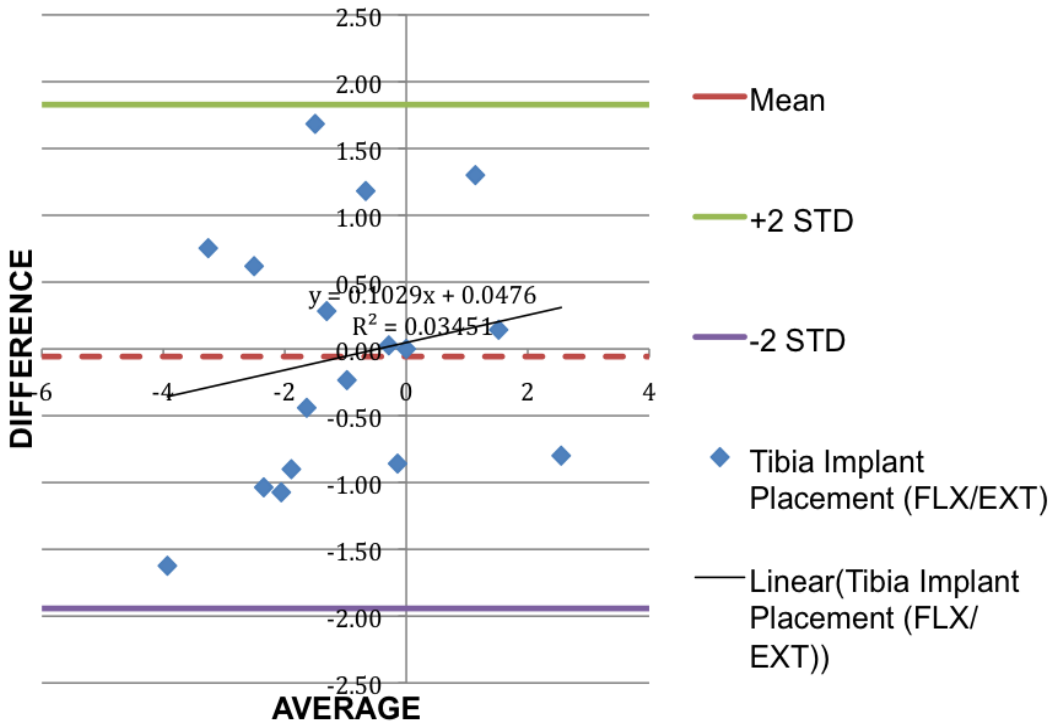

Figure 2-15. Bland Altman plot of tibia implant placement in FLX/EXT rotation.

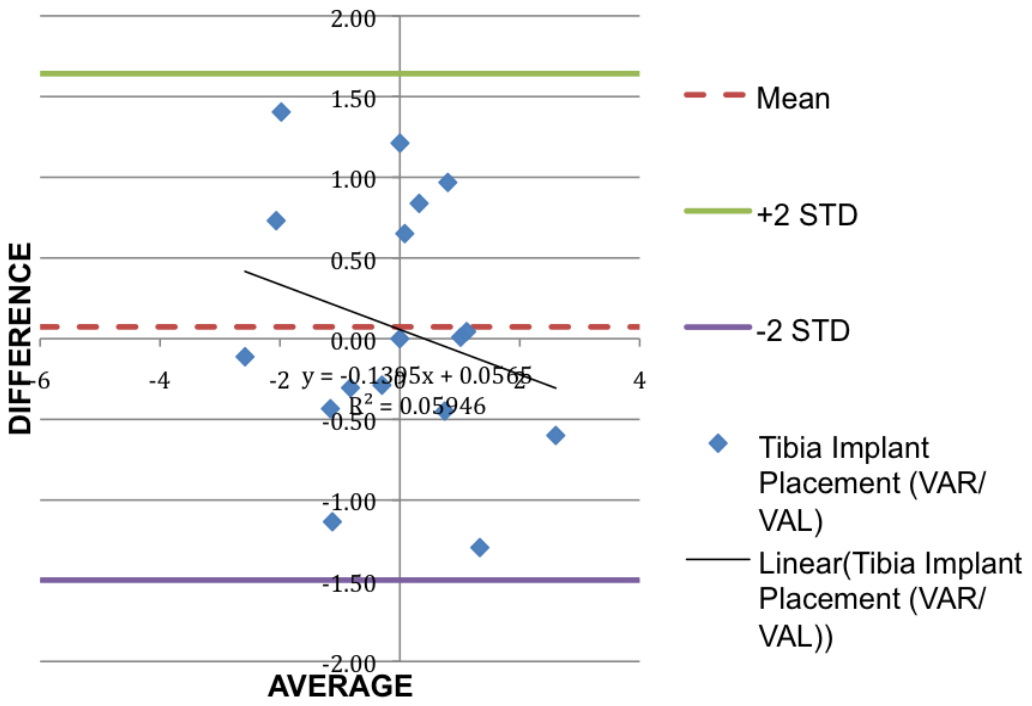

Figure 2-16. Bland Altman plot of tibia implant placement in VAL/VAL rotation.

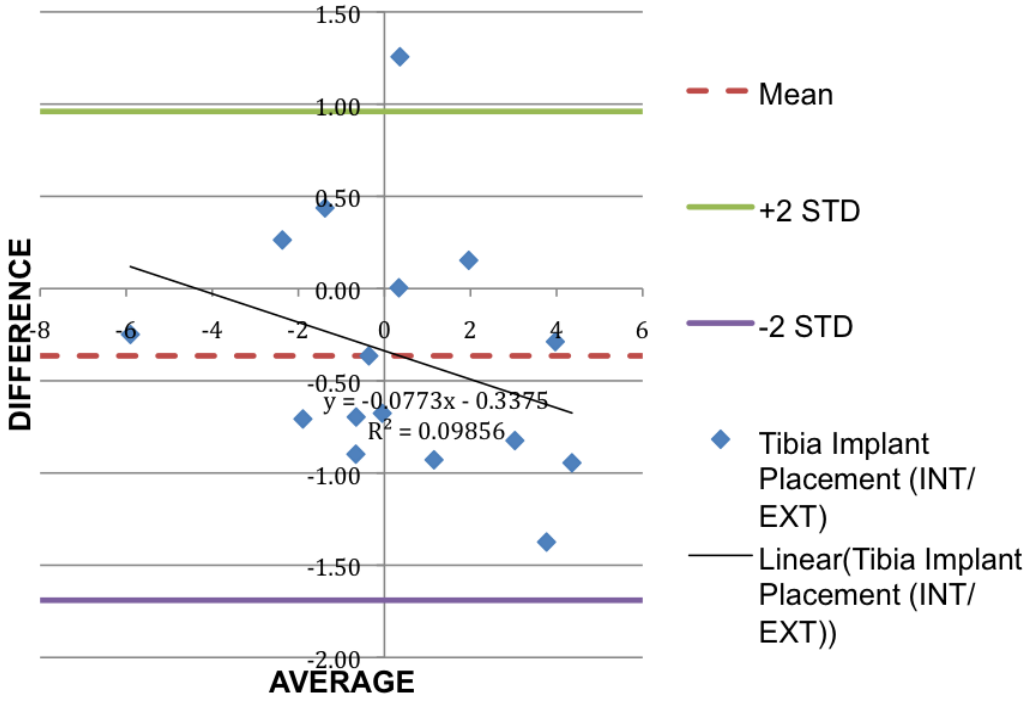

Figure 2-17. Bland Altman plot of tibia implant placement in INT/EXT rotation.

APPENDIX
MI AND OPTIMIZER PARAMETER VALUES

Table A-1. ITK Mattes MI metric parameter values.

Parameters	Value
Use all pixels	On
Use Explicit PDFDerivatives	On
Number of Spatial Samples	8000
Number of Histogram Bins	2000

Table A-2. ITK Amoeba optimizer parameter values.

Parameters	Value
Automatic initial simplex	On
Initial simplex delta	5
Maximum number of Iterations	2000
Parameters convergence tolerance	0.25
Function convergence tolerance	0.0005
Optimizer	Minimize

LIST OF REFERENCES

Andronach A., Siebentahl M., Szekely G. and Cattin P. 2008. Non-rigid registration of multi-modal images using both mutual information and cross-correlation. Medical Image Analysis 12:2-15.

Betke M., Hong H. and Ko J. 2001. Automatic 3D Registration of Lung Surfaces in Computed Tomography Scans. MICCAI LNCS 2208:725-733.

Bland JM, Altman DG (1986) Statistical method for assessing agreement between two methods of clinical measurement. The Lancet 327(8476):307-310

Brown L. 1992. A survey of image registration techniques. ACM Computing Surveys 24(4):326–376.

Brown L. and Boult T. 1996. Registration of planar film radiographs with computed tomography. Proc. MMBIA 42-51.

Butz T and Thrian JP. 2001. Affine Registration with Feature Space Mutual Information. MICCAI LNCS 2208:549-556.

Cizek J., Herholz K., Vollmar S., Schrader R., Klein J. and Heiss WD. 2004. Fast and robust registration of PET and MR images of human brain. NeuroImage 22(1):434-442.

Fueziec A., Kazanzide P., Williamson B., Taylor R. and Lord D. 1998. Anatomy-based registration of CT-Scan and X-ray Fluoroscopy data for intra-operative guidance of a surgical robot. Proc. SPIE Medical Imaging 81-94.

Harber E. and Modersitzki J. 2006. Intensity gradient based registration and fusion of multi-modal images. MICCAI LNCS 4191:726-733.

Holden M., Hill D., Denton E., Jarosz J., Cox T., Rohlfing T., Goodey J. and Hawkes D. 2000. Voxel Similaritey Measures for 3-D Serial MR Brain Image Registration. IEEE Transactions on Medical Imaging 19(2):94–102.

Ibanez L., Schroder W., Ng L. and Cates J. 2005. The ITK Software Guide Second Edition *Updated for ITK version 2.4.* www.itk.org.

Kern F. and Pattichis M. 2007. Robust Multispectral Image Registration Using Mutual-Information Models. IEEE Transactions on Geoscience and Remote Sensing 45(5):1494-1505.

Klein S., Staring M., Murphy K., Vergever M and Pluim J. 2010. elastix: A Toolbox for Intensity-Based Medical Image Registration. IEEE Transactions on Medical Imaging 29(1):196–205.

Lagarias J., Reeds J., Wright M. and Wright P. 1998. Convergence properties of the Nelder-Mead simplex method in low dimensions. SIAM Journal on Optimization 9(1):112-147.

Lemieux L., Jagoe R., Fish D., Kitchen N. and Thomas D. 1994. A patient-to-computed-tomography image registration method based on digitally reconstructed radiographs. American Association of Physicists in Medicine 21(11):1749-1760.

Maes F., Collignon A., Vandermeulen D., Marchal G. and Suetens P. 1997. Multimodality image registration by maximization of mutual information. IEEE Transactions on Medical Imaging 16(2):187-198.

Maintz J. and Viergever M. 1998. A survey of medical image registration. Medical Image Analysis 92(1):1-36.

Mattes D., Haynor D., Vesselle H., Lewellen T. and Eubank W. 2003. PET-CT Image Registration in the Chest Using Free-Form Deformations. IEEE Transactions on Medical Imaging 22(1):120–128.

Maurer Jr. C., Aboutanos G., Dawant B., Maciunas R. and Fitzpatrick J. 1996. Registration of 3-D Images Using Weighted Geometrical Features. IEEE Transactions on Medical Imaging 175(6):836–849.

McKinnon K. 1998. Convergence of the Nelder-Mead simplex method to a nonstationary point. SIAM Journal on Optimization 9(1):148-158.

Nelder J. and Mead R. 1965. A simplex method for function minimization. Computer Journal 7:308-313.

Patil S and Ravi B. 2005. Voxel-based representation, display and thickness analysis of intricate shapes. Ninth International Conference on Computer Aided Design and Computer Graphics.

Penney G., Weese J., Little J., Desmedt P., Hill D. and Hawkes D. 1998. A Comparison of Similarity Measures for Use in 2-D-3-D Medical Image Registration. *IEEE Transactions on Medical Imaging* 17(4):586–595.

Pluim J., Maintz J and Viergever M. 2000. Image Registration by Maximization of Combined Mutual Information and Gradient Information. MICCAI LNCS 567-578.

Pluim J., Maintz J. and Viergever M. 2003. Mutual-information-based registration of medical images: A survey. IEEE Transactions on Medical Imaging 22(8):986–1004.

Rasband W.S., 2003. ImageJ, National Institutes of Health, Bethesda, http://rsb.info.nih.gov/ij/,.

Roche M., O'Loughlin PF., Kendoff D., Musahl V. and Pearle AD. 2009. Robotic arm-assisted unicompartmental knee arthroplasty: preoperative planning and surgical technique. American Journal of Orthop 38(2S):10-15.

Shams R., Sadeghi P., Kennedy R. and Hartley R. Parallel 2010. computation of mutual information on the GPU with application to real-time registration of 3D medical images. Computer Methods and Programs in Biomedicine 99:133-146.

Studholme C., Hill D. and Hawkes D. 1996. Automated 3-D registration of MR and CT images of the head." Medical Image Analysis 1(2):163-175.

Thirion JP. and Calmon G. 1999. Deformation Analysis to Detect and Quantify Active Lesions in Three-Dimensional Medical Image Sequences. IEEE Transactions on Medical Imaging 28(5):429–441.

Viola P. and Wells III W. 1995. Alignment by maximization of mutual information. International conference on computer vision 16–23.

Viola P. and Wells III W.M. 1997. Alignment by maximization of mutual information. International Journal of computer vision 24(2):137–154.

Zitova B. and Flusser J. 2003. Image registration methods: a survey. Image Vision Computing 21(11):977-1000.

BIOGRAPHICAL SKETCH

Brian Park received his bachelor's degree from University of North Carolina at Charlotte, in 2008. He joined the University of Florida in the fall of 2009. Apart from his pursuit in Biomechanical Engineering, his biggest interest lies in sports automobiles.